Interaction of an Optical Soliton with a Dispersive Wave

A. Efimov,[1] A. V. Yulin,[2] D. V. Skryabin,[2] J. C. Knight,[2] N. Joly,[2] F. G. Omenetto,[3] A. J. Taylor,[1] and P. Russell[2]

[1]*Materials Science and Technology Division, MST-10, Los Alamos National Laboratory, Los Alamos, New Mexico 87545, USA*
[2]*Centre for Photonics and Photonic Materials, Department of Physics, University of Bath, Bath BA2 7AY, United Kingdom*
[3]*Department of Biomedical Engineering and Department of Physics, Tufts University, Medford, Massachusetts 02155, USA*

(Received 4 August 2005; published 15 November 2005)

Scattering of a dispersive wave by optical solitons is studied experimentally in photonic crystal fibers in cases when the soliton and the dispersive wave have either identical or orthogonal polarization states. Observations of new resonant frequencies are reported. The experimental results are compared to numerical simulations and predictions from the recently derived wave vector matching conditions.

DOI: 10.1103/PhysRevLett.95.213902 PACS numbers: 42.81.Dp, 42.65.Ky, 42.65.Tg

Sufficiently strong excitation of a nonlinear system often naturally evolves into a mixture of nondispersive localized wave packets, called solitary waves or simply solitons, embedded into a sea of small-amplitude dispersive waves. Thus, the interaction between solitons and coexisting dispersive waves is one of the long-standing problems in nonlinear wave dynamics [1]. An obvious example is that of water-wave solitons traveling through small-amplitude ripples [2]. Another example directly relevant in the context of this work comes from fiber optics. Namely, an intense ultrashort optical pulse propagating in an optical fiber can break up into a sequence of solitons immersed into linear dispersive waves also generated during this process; see, e.g., [3–7] for recent observations of this effect. The pulse breakup and subsequent nonlinear interaction of the emergent waveforms lead to a significant spectral broadening or to supercontinuum generation [3–7].

To understand the details of the supercontinuum generation in optical fibers, it is natural to consider separately the radiation of dispersive waves by individual solitons (see, e.g., [3,8,9]) and scattering of dispersive waves by solitons [10]. It has been predicted that scattering of linear waves from optical fiber solitons in the presence of significant higher-order dispersion leads to the generation of new spectral components [10]. The phase matching conditions that describe this process are qualitatively distinct from those applicable to the four-wave mixing (FWM) of dispersive waves only, i.e., without solitons [11]. Some features of the recent experiments on supercontinuum generation [5,6] in photonic crystal fibers (PCFs) pumped with short pulses can be interpreted using the theory of Ref. [10].

The scattering of linear dispersive waves from spatially localized soliton structures has also been considered in the context of Bose-Einstein condensates [12] and in modulated planar optical waveguides [13]. The focus of these two papers, however, has been on the calculation of reflection and transmission properties of the potential created by the soliton, and the possibility of generating new spectral components has not been considered. There has also been a series of earlier papers [14] analyzing the interaction of solitons with dispersive waves in the integrable idealization of the nonlinear Schrödinger (NLS) model, where no harmonic generation from this process is possible due to the robustness of the single soliton solutions within the ideal NLS equation.

The main purpose of this work is to present the results of experiments which directly test the interaction of fiber solitons with a continuous wave (CW). Both the solitons and the CW were launched into the fiber separately and in a controlled manner. This setup allowed us independent control of the powers and the central wavelengths of the interacting waves, as well as their polarizations.

Fiber appropriate for our purposes ideally should have a sufficiently high nonlinear coefficient and a large group velocity dispersion slope. The former is important to observe nonlinear interactions using available laser sources, and the latter is required to have a system which is far from the integrable limit, where frequency conversion with solitons is forbidden [14]. A small-core photonic crystal fiber satisfies both of the above requirements. The PCF used in this work is the same as the one used in Ref. [6]. In this PCF, there are two wavelengths ($\lambda_1 = 680$ nm, $\lambda_2 = 1510$ nm), where the group velocity dispersion (GVD) is zero. For $\lambda_1 < \lambda < \lambda_2$, the GVD is anomalous and it is normal otherwise. Working in the proximity of λ_2 gives access to the much steeper GVD slope. The fiber core size (of the order of the wavelength) provides a large value for the nonlinear coefficient $\gamma \simeq 0.1\ (\mathrm{Wm})^{-1}$ [6,11]. The length of the fiber used in our experiments is 90 cm. The source for the solitons in the fiber is a synchronously pumped optical parametric oscillator, which generates a train of 100 fs pulses at 80 MHz repetition rate and central wavelength of 1425 nm. The CW field at 1546 nm is generated by a temperature-controlled laser diode and amplified with an erbium-doped fiber amplifier. The CW signal is thus located in the normal dispersion region, and the power coupled to the fiber is estimated at 0.1 W.

For the numerical model, we use the generalized vector NLS equations [7]:

$$-i\partial_z A_{x,y} = D_{x,y}(i\partial_t)A_{x,y} + \gamma\left[|A_{x,y}|^2 + \frac{2}{3}|A_{y,x}|^2\right]A_{x,y} + A_{x,y}\int_{-\infty}^{+\infty} R(t')I(t-t',z)dt', \quad I = |A_x|^2 + |A_y|^2. \tag{1}$$

Crucially important terms in the dispersion operators $D_{x,y}(i\partial_t) = \beta_{x,y}^{(1)} i\partial_t + \beta_{x,y}^{(2)}/2!\,(i\partial_t)^2 + \beta_{x,y}^{(3)}/3!\,(i\partial_t)^3 + \ldots$ are the group velocity $\sim\beta_{x,y}^{(1)}$, group velocity dispersion $\sim\beta_{x,y}^{(2)}$, and third-order dispersion $\sim\beta_{x,y}^{(3)}$. The higher-order dispersion terms up to 7th order have also been included in our modeling to match the experimentally measured dispersion profile of the fiber. The measured group delay between the two eigenpolarizations of the PCF is $|\beta_x^{(1)} - \beta_y^{(1)}| \simeq 1.4$ ps/m at 1425 nm. The differences between the second- and higher-order dispersions for two eigenpolarizations could not be resolved experimentally: $\beta_{x,y}^{(2)} \simeq -72$ ps^2/km and $\beta_{x,y}^{(3)} \simeq -0.65$ ps^3/km at 1425 nm. The difference between the refractive indices of the two principal polarization axes has been estimated at 7×10^{-4} by numerical modeling. This corresponds to a beat length $\simeq$ 2 mm, which is much less than the dispersion length of 14 cm at 1425 nm and the walkoff length of 7 cm due to the difference in the group velocities. Therefore, the influence of the terms proportional to $A_{x,y}^* A_{y,x}^2$ on the field dynamics is negligible [11], and they have not been included into Eqs. (1). The function $R(t)$ entering the integral in Eq. (1) is the standard Raman response [11].

First we describe experimental results for the case when the soliton and CW pump have the same polarizations (see Ref. [10] for the corresponding theory). To analyze the output signal, we use cross-correlation frequency resolved optical gating (XFROG) spectrograms, simultaneously showing spectral and temporal content of the signal [4–6,15]. Our experimental and numerical results are shown in Fig. 1. The peak pump power is 1.7, 4.4, and 7 kW for the 1st, 2nd, and 3rd columns in Fig. 1, respectively. The bottom row in Fig. 1 shows experimental XFROGs for the case when no CW pump has been launched into the fiber. From the two top rows, one can see that as the soliton power increases its interaction with the CW radiation becomes more and more pronounced. There are two reasons for this. The first is that, in all the cases considered in this work, the FWM term responsible for the interaction between the soliton and CW pump is proportional to the modulus squared of the soliton field and only to the first power of the (unconjugated) CW field [10]. Second, and more important, is that, with the increase of the pump power, the soliton becomes narrower in the time domain, and, therefore, the Raman effect brings the soliton carrier frequency closer to the CW frequency, which strongly enhances the efficiency of the FWM process [10]. Comparison of theoretical and experimental results unambiguously indicates that the frequency component to the longer wavelength side of the CW line in Figs. 1(d) and

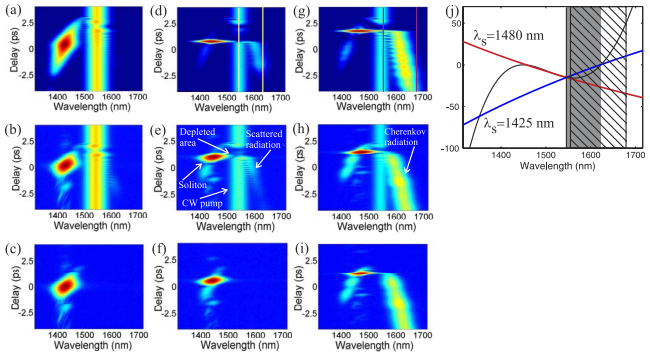

FIG. 1 (color online). Interaction between the soliton and CW having the same polarizations. First row (a),(d),(g) numerical modeling, and second row (b),(e),(h) experimental measurements, showing XFROG diagrams resulting from the interaction between the soliton and CW. Third row (c),(f),(i) shows experimental measurements with the CW field switched off. 1st, 2nd, and 3rd columns correspond to the soliton peak power 1.7, 4.4, and 7 kW, respectively. Propagation length is 90 cm and CW power is 0.1 W for all the panels. Panel (j) shows the graphical solution to the wave vector matching condition (2) for the two values of the soliton wavelength λ_s. The shaded gray area shows the FWM band, and the dashed area shows the Cherenkov band. The dashed vertical line marks the zero GVD wavelength. The color scale used in spectrograms is logarithmic.

1(e) is generated as a result of the FWM between the soliton and the CW pump. When the CW pump is switched off [Fig. 1(f)], the FWM signal disappears. Another important observation which we make from this part of our work is the appearance of the hole in the CW pump; see Figs. 1(e) and 1(h). This hole is formed because the energy taken from the CW pump is transferred (scattered) by the soliton to the new spectral component.

The wave vector matching condition for the FWM process between the soliton and the CW relevant to our experiments is [10]

$$k_{s/\mathrm{signal}} + \beta_{\mathrm{cw}} - k_{s/\mathrm{cw}} = \beta_{\mathrm{signal}}, \tag{2}$$

where β_{cw} and β_{signal} are the propagation constants of the fiber mode taken for the frequency of the CW pump and for the frequency of the generated signal. $k_{s/\mathrm{signal}}$ and $k_{s/\mathrm{cw}}$ are the wave vectors of the Fourier harmonics of the soliton at the signal frequency and at the CW frequency, respectively. This condition predicts the frequency of the newly generated peak very well. Conveniently normalized and rescaled geometrical representation of the wave vector matching (2) is shown in Fig. 1(j), where the nearly straight lines represent the left-hand side of Eq. (2) for the two different values of the soliton wavelength, and the curved line is the right-hand side of Eq. (2). Since the soliton wavelength is being shifted by the Raman effect, the matching point of the FWM process also shifts with both propagation distance and pump power. The shaded region in Fig. 1(j) and the white lines in Fig. 1(d) show the boundaries of the FWM band. Efficiency of excitation of the other FWM

resonances located on the left from the shaded region is low, and they are not observed in the experiment.

When we attempted to increase the pump power further and make the FWM peak brighter, we encountered a problem. For higher pump powers, the soliton shifts further towards the point where its frequency is stabilized (approximately at 1480 nm) due to spectral recoil [8]. The frequency stabilization process is accompanied by strong emission of Cherenkov radiation, which is matched for $k_{s/\mathrm{signal}} = \beta_{\mathrm{signal}}$ and spreads over the spectral range, where, for smaller powers, we observed the FWM signal [see the overlap between the dashed and shaded regions in Fig. 1(j)]. Comparison of Figs. 1(g)–1(i) clearly shows that this strong radiation is indeed the Cherenkov one, because its emission occurs independently of the CW pump. Thus, in the case when the soliton and CW pump have the same polarizations, observation of the newly generated wave can be achieved only for a relatively small power range of the soliton pump.

Equation (2) can be equally applied to the case when the soliton and CW are orthogonally polarized and launched in the corresponding eigenaxis of the fiber. The polarization of the FWM signal coincides with the CW polarization, while Cherenkov radiation always has the same polarization as the soliton. Thus, performing measurements with orthogonally polarized soliton and CW, one can hope not only to uncover the new features of the FWM process but also to separate the FWM signal from the Cherenkov radiation. In the remaining part of the work, we describe our measurements carried out with orthogonally polarized solitons and CW radiation.

XFROG spectrograms measured in the polarization corresponding to the soliton part of the field are very similar to those presented in Figs. 1(c), 1(f), and 1(i). The orthogonally polarized field containing the CW pump, however, develops different spectral and temporal features; see Figs. 2 and 3. It is important, for the subsequent discussion, that throughout the relevant frequency interval the group velocity at one polarization, let us say x, is larger than the group velocity of the y-polarized light.

Figure 2 corresponds to the situation when the soliton group velocity is larger than the group velocity at the CW frequency. The measurements shown in Fig. 2(d) are reproduced by the two different numerical results shown in Figs. 2(e) and 2(f). In Fig. 2(e) none of the solitons couple to the CW polarization, while in Fig. 2(f) 0.3% of the input power of the short pulsed pump is coupled into the second polarization to model experimental imperfections in launching the light into the fiber. The radiation pattern on the left of the CW pump seen in Fig. 2(d) is explained by this imperfection. The soliton frequency changes linearly with propagation distance due to the Raman effect, and the FWM signal is continuously generated in the course of the propagation. This implies that the frequency of the FWM resonance visible in the XFROGs also must vary linearly with delay; see Figs. 2(d)–2(f). Using Eq. (2), we predict generation of the FWM signal in the shaded interval shown in the wave vector matching diagram in Fig. 2(a) [see also the white lines in Fig. 2(e)].

Radiation emitted due to parasitic coupling of the soliton to the CW polarization forms its own continuum. This continuum is emitted at the very beginning of the fiber [see Fig. 2(c)], and, with further propagation, its spectral components propagate with their own group velocities, which results in the parabolic shape of the corresponding signal in the XFROG spectrogram; see Figs. 2(c) and 2(f). The

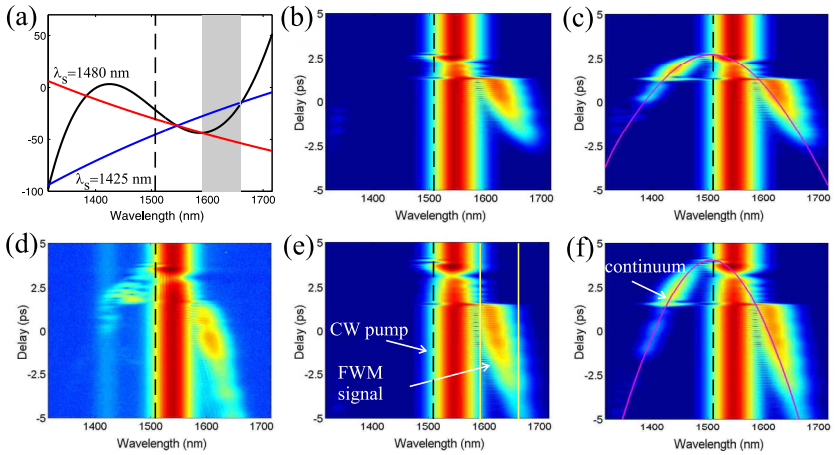

FIG. 2 (color online). Interaction between the orthogonally polarized soliton and CW. Soliton group velocity is greater than the group velocity at the CW frequency. (a) The graphical solution to the wave vector matching condition (2) for the two values of the soliton wavelength λ_s. The grey shaded region marks the FWM band. The dashed vertical line marks the zero GVD wavelength. (d) Experimentally measured XFROG in the CW polarization at the end of the 90 cm fiber and the soliton peak power 10 kW. (b),(c),(e),(f) Numerically computed XFROGs. (b),(c) and (e),(f) correspond to the 45 and 90 cm propagation length, respectively. (b),(e) correspond to the case when zero fraction of the soliton pump couples to the CW polarization, and (c),(f) correspond to the case when 0.3% of the soliton pump power couples to the CW polarization. The color scale used in spectrograms is logarithmic.

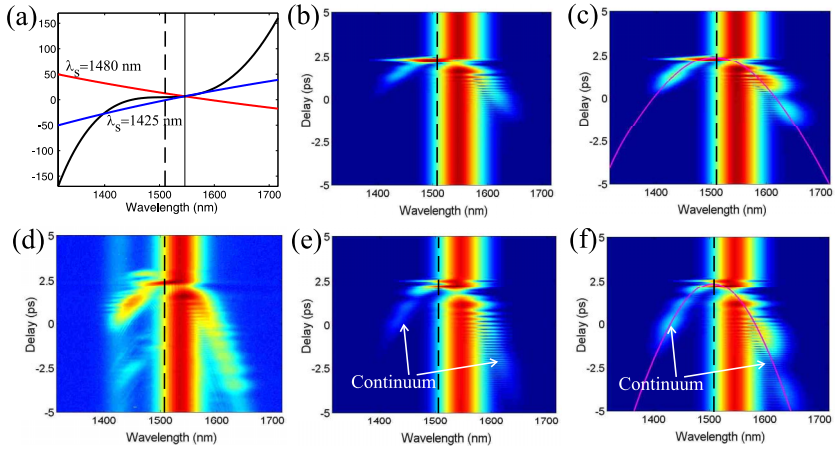

FIG. 3 (color online). Interaction between the orthogonally polarized soliton and CW, but soliton and CW polarizations are interchanged relative to Fig. 2, i.e., soliton group velocity is less than the group velocity at the CW frequency. (a) shows that the wave vector matching condition (2) does not produce FWM band as in the case in Fig. 2(a). The dashed vertical line marks the zero GVD wavelength. XFROG diagrams in (b)–(f) are measured and calculated for the same parameters as in Fig. 2. The color scale used in spectrograms is logarithmic.

parabola shown in Figs. 2(c) and 2(f) is calculated as $\tau = (\partial\beta_{\mathrm{cw}}/\partial\omega)z$. Comparing Figs. 2(b) and 2(c) with Figs. 2(e) and 2(f), one can see that the depletion area inside the CW and the length of the FWM signal are increasing with propagation. This and detailed analysis of XFROG images taken for multiple values of z indicate that in this case there is a continuous energy transfer from the CW into the resonant radiation along the entire fiber length.

If we swap polarizations of the soliton and CW, then the scattering process generates a different set of XFROG traces, as shown in Fig. 3. In this case, the soliton group velocity is smaller than the CW-group velocity, and Eq. (2) predicts no FWM resonances for the relevant soliton frequencies; see the wave vector matching diagram in Fig. 3(a). The parabolic radiation pattern observed in the experiment is well reproduced if we couple 0.3% of the short pulsed pump into the CW polarization. However, in this case a weaker continuum is generated even if no soliton pump is coupled to the CW polarization; see Fig. 3(e). Note that, in this case, the CW depletion area hardly changes with z; see Figs. 3(b), 3(c), 3(e), and 3(f). This indicates that the energy is transferred from the CW field into the continuum only at the beginning of the fiber, and, after this, no further continuum is generated, but it simply disperses.

In summary, we have carried out an experimental investigation of the interaction of an optical fiber soliton with a dispersive wave. We have observed generation of new frequencies resulting from this process, which confirmed recent theoretical predictions of the differences distinguishing the FWM of the dispersive waves with nondispersive soliton pulses from the FWM of all-dispersive waves [10]. We have also demonstrated that, when the FWM process is not phase matched, interaction of the orthogonally polarized CW and soliton results in the continuum generation in the CW polarization.

[1] V. E. Zakharov *et al.*, Physica (Amsterdam) **152D**, 573 (2001).
[2] E. Infeld and G. Rowlands, *Nonlinear Waves, Solitons and Chaos* (Cambridge University Press, Cambridge, England, 1990).
[3] J. Herrmann *et al.*, Phys. Rev. Lett. **88**, 173901 (2002).
[4] J. M. Dudley *et al.*, Opt. Express **10**, 1215 (2002).
[5] T. Hori, N. Nishizawa, T. Goto, and M. Yoshida, J. Opt. Soc. Am. B **21**, 1969 (2004); G. Genty, M. Lehtonen, and H. Ludvigsen, Opt. Express **12**, 4614 (2004).
[6] A. Efimov *et al.*, Opt. Express **12**, 6498 (2004).
[7] F. Lu *et al.*, Phys. Rev. Lett. **93**, 183901 (2004).
[8] D. V. Skryabin *et al.*, Science **301**, 1705 (2003); F. Biancalana, D. V. Skryabin, and A. V. Yulin, Phys. Rev. E **70**, 016615 (2004).
[9] P. K. A. Wai, H. H. Chen, and Y. C. Lee, Phys. Rev. A **41**, 426 (1990); J. N. Elgin, Phys. Rev. A **47**, 4331 (1993); V. I. Karpman, Phys. Rev. E **47**, 2073 (1993).
[10] A. V. Yulin, D. V. Skryabin, and P. St. J. Russell, Opt. Lett. **29**, 2411 (2004); D. V. Skryabin and A. V. Yulin, Phys. Rev. E **72**, 016619 (2005).
[11] G. P. Agrawal, *Nonlinear Fiber Optics* (Academic, San Diego, CA, 2001).
[12] P. O. Fedichev, A. E. Muryshev, and G. V. Shlyapnikov, Phys. Rev. A **60**, 3220 (1999).
[13] S. Flach *et al.*, Phys. Rev. Lett. **95**, 023901 (2005).
[14] N. Akhmediev and S. Wabnitz, J. Opt. Soc. Am. B **9**, 236 (1992); E. A. Kuznetsov, A. V. Mikhailov, and I. A. Shimokhin, Physica (Amsterdam) **87D**, 201 (1995).
[15] A. Efimov and A. J. Taylor, Appl. Opt. **44**, 4408 (2005).